RSC Advances

PAPER

View Article Online
View Journal | View Issue

Cite this: *RSC Adv.*, 2025, **15**, 36365

Rapid synthesis of phosphomolybdic acid encapsulated ZIF-8 for efficient uranium(VI) capture from alkaline solution

Abdelaal S. A. Ahmed, *[a] El Sayed A. Haggag,[b] Mohamed F. Cheira,[b] Ahmed A. Abdelsamad[b] and Ashraf M. Abdel-lateef[c]

Received 10th September 2025
Accepted 13th September 2025

DOI: 10.1039/d5ra06854a

rsc.li/rsc-advances

Phosphomolybdic acid hydrate (PMA) encapsulated within a ZIF-8 framework (PMA@ZIF-8) was synthesized and utilized for U(VI) adsorption from the alkaline leach liquor of dolostone material collected from SW Sinai. The prepared PMA@ZIF-8 composite was characterized by FT-IR, XRD, XPS, and SEM techniques to confirm its structural and morphological properties. To estimate the optimum conditions for the removal of U(VI), various parameters including pH, contact time, solid/liquid ratio, initial U(VI) concentration, and temperature were examined in a batch adsorption technique. The maximum adsorption capacity of the PMA@ZIF-8 composite toward U(VI) was achieved at pH 10.5 after 90 min at room temperature. The kinetic study demonstrated that the adsorption of U(VI) onto the PMA@ZIF-8 composite fitted well with the pseudo-second-order model, and adsorption isotherm results indicated that the U(VI) adsorption fitted the Langmuir model. Thermodynamic analysis suggested that the adsorption is an exothermic process. This study reveals the potential use of the PMA@ZIF-8 adsorbent for the removal of U(VI) from alkaline leach liquor solutions of dolostone ore.

1 Introduction

Nuclear energy plays an important role in sustainable development. The principal nuclear fuel, uranium (U), is relatively abundant in the continental crust.[1] Uranium exists in several oxidation states in nature, but the hexavalent state, U(VI), is the most stable and common. U(VI) is usually found as the uranyl ion (UO_2^{2+}), which is highly toxic. Because of its strategic importance in nuclear energy and its role as an environmental hazard, U(VI) recovery is a crucial component of future nuclear energy cycles. During uranium mining and processing, vast amounts of radioactive effluents are generated, which often contain U(VI) concentrations below 1.0 mg L^{-1}. These effluents, if discharged, can contaminate groundwater and surface water.[2] Even at trace levels, U(VI) can accumulate in aquatic organisms and humans, inducing damage to the liver, spleen, lungs, and bone marrow.[3] Therefore, U(VI) recovery has long been a target of environmental remediation and water purification.[4,5]

Commercial uranium recovery is almost exclusively based on alkaline leaching processes with sodium carbonate or sodium bicarbonate solutions, in which uranium exists as the soluble and stable uranyl tricarbonate complex $[UO_2(CO_3)_3]$.[4–6] Alkaline leaching is a highly selective process, as most of the associated metals are not soluble under these conditions. Therefore, the leach liquor produced is relatively pure, recyclable, and associated with less corrosion issues.[7,8] Different techniques have been utilized for uranium recovery from such alkaline leach liquors, including direct precipitation, ion-exchange resins, membrane separation,[9] solvent extraction and adsorption.[10,11] The choice of method depends on the leach medium, uranium concentration, co-dissolved impurities, and the desired product purity.

Uranium mineralization in Egypt is widely distributed, particularly in dolostone ores of the Um Bogma area, southwestern Sinai. The area, which is situated to the east of Abu Zeneima on the Gulf of Suez, is overlain by Paleozoic sediments that unconformably overlie Precambrian basement rocks.[12] Dolostone, a calcium–magnesium carbonate rock ($CaMg(CO_3)_2$), is the dominant host. It is typically formed by diagenetic substitution of Ca by Mg in limestone, which is favored in ancient formations.[13] Adsorption is considered a highly promising technique for uranium recovery due to its low cost, simplicity, and efficiency.[14] However, most of the sorbents can operate optimally at pH < 8.5.[14,15] At acidic pH, U(VI) exists mainly as UO_2^{2+}, whose complexation with O-, N-, or P-donor ligands (*e.g.*, amidoxime, amine, phosphonate, carboxylate) is facile.[15,16] Accordingly, such functional groups are prevalent in sorbent design. At high pH, however, UO_2^{2+} hydrolyzes and polymerizes to give anionic uranyl species (*e.g.*, $(UO_2)_2(OH)_4$, $UO_2(OH)_3^-$, $UO_2(OH)_4^{2-}$).[17] Electrostatic repulsion between anionic uranyl species and deprotonated sorbent

[a]*Chemistry Department, Faculty of Science, Al-Azhar University, Assiut 71524, Egypt. E-mail: abdelaalsaiyd@azhar.edu.eg*

[b]*Nuclear Materials Authority, P.O. Box 530, Maadi, Cairo, Egypt*

[c]*Accelerations and Ion Sources Department, Central Laboratory for Elemental and Isotopic Analysis, NRC, Egyptian Atomic Energy Authority, Cairo, 13759, Egypt*

functional groups significantly impedes adsorption efficiency.[18] Consequently, alkaline solutions are typically acidified prior to U(VI) recovery, which increases costs and exacerbates radioactive hazards.

Recent porous materials have demonstrated the ability to uptake many materials, including radioactive hazards species from the environment.[19–21] In the last decade, metal–organic frameworks (MOFs), particularly ZIF-8, have shown promising applications in pollutant remediation.[22] MOFs possess ultra-high porosity, tunable chemistry, and stability that make them excellent candidates for radionuclide capture.[23,24] ZIF-8 functionalization has attained record uranium uptake capacities. For instance, a hierarchical porous ZIF-8 functionalized with salicylaldoxime and polydopamine (H-PDA/SA-ZIF-8) displayed an adsorption capacity of 869.6 mg g^{-1}, with equilibrium reached in just 20 min, and demonstrated effective uranium removal from natural seawater (~6.9 mg g^{-1} after 15 days).[25] Chitosan/ZIF-8 beads, similarly, demonstrated a high adsorption capacity of ~629 mg g^{-1} and good recyclability.[26] These advancements underline the potential of MOF-based sorbents but with the shortcoming of their performance under alkaline conditions, where uranyl species exist predominantly in the form of anionic complexes.

Mechanistic studies highlight that uranium adsorption on MOFs is mainly governed by coordination interactions and inner-sphere complexation with their functional groups, sometimes assisted by electrostatic attraction.[27] Amidoxime, carboxyl, amine, and phosphoryl functional groups were found to significantly enhance uranium selectivity.[28] Selective and efficient U(VI) recovery directly from alkaline media remains a challenge. Herein, we report for the first time a simple synthesis of phosphomolybdic acid embedded in ZIF-8 (PMA@ZIF-8) as a sorbent for the uptake of U(VI) from alkaline solutions. The synergetic contribution of the porosity and high surface area of ZIF-8 and the high affinity of uranyl ions for phosphorus-rich heteropolyacids is responsible for the promising performance of this composite. Our findings demonstrate that encapsulation of heteropolyacids in MOFs is a viable strategy for the creation of next-generation adsorbents for uranium remediation under alkaline conditions.

2 Experimental section

2.1 Materials

Sodium hydroxide (NaOH, ≥98%, anhydrous), phosphomolybdic acid hydrate (PMA; $H_3PMo_{12}O_{40}\cdot xH_2O$, 99.99% trace metals basis), hydrochloric acid (HCl, 37%), zinc acetate dihydrate ($Zn(CH_3COO)_2\cdot 2H_2O$, ≥98%), 2-methylimidazole ($C_4H_6N_2$; Mwt 82.10 g mol^{-1}), hydrochloric acid (HCl, ≥36%), sulfuric acid (H_2SO_4, ≥98%), nitric acid (HNO_3, ≥69%), sodium carbonate (Na_2CO_3; powder, ≥99.5%), sodium chloride (NaCl, ≥99.0%), sodium sulphate (Na_2SO_4), sodium acetate (CH_3COONa) and absolute ethanol (C_2H_6O, ≥99.9%) were purchased from Sigma-Aldrich. All reagents were of analytical purity and used without further purification. All preparations in our study were performed using distillated water obtained from an ultra-pure purifier (Ulupure, resistivity ≥ 18.2 MΩ).

2.2. Preparation of carbonate leach liquor

The dolostone ore sample under study was collected from SW Sinai, pulverized, and thoroughly mixed by quartering to achieve homogeneity. It was then submitted to a thorough chemical examination using atomic spectrometry to determine its principal oxide contents as well as a few trace elements. For the experiment, 200 g of the pulverized ore sample was treated with a (3 : 1) mixture of Na_2CO_3 and $NaHCO_3$ with 5 mL of H_2O_2, and the mixture was continuously stirred for 2 h at room temperature. After filtering the resultant slurry, the residue was cleaned, and uranium uptake from alkaline leach liquor by PMA@ZIF-8 was conducted. Leaching of uranium from a technological sample (400 mg L^{-1}) in SW Sinai of Um Bogma formation was carried out using a mixture of sodium carbonate/sodium bicarbonate in the presence of an oxidant, as shown by chemical equations (eqn (1)–(4)). The ICP chemical analysis of dolostone material from SW Sinai of Um Bogma is shown in Table 1.

$$UO_2^{2+} + CO_3^{2-} \leftrightarrow UO_2CO_3 \quad (1)$$

$$UO_2CO_3 + CO_3^{2-} \leftrightarrow UO_2(CO_3)_2^{2-} \quad (2)$$

$$UO_2(CO^3)_2^{2-} + CO_3^{2-} \leftrightarrow UO_2(CO_3)_3^{4-} \quad (3)$$

$$2UO_2 + O_2 \leftrightarrow 2UO_3 \quad (4)$$

2.3 Preparation of PMA@ZIF-8 adsorbent material

In our study, PMA@ZIF-8 composite was prepared in successive two steps as illustrated in Fig. 1. First, ZIF-8 nanocrystals were prepared using DI water as the solvent for ZIF-8 resources as previously reported.[29] Typically, 10 mL an aqueous solution containing 0.22 g of Zn-acetate added stepwise to an aqueous solution of 4 g of 2-methylimidazole dissolved in 70 mL distillated water under magnetic stirring for 2 h at room temperature until a milky-like ZIF-8 suspension was obtained. The second step is the impregnation of phosphomolybdic acid hydrate (PMA) onto ZIF-8 particles. Exactly 0.3 g of PMA was slowly added to the milky-like ZIF-8 suspension in water. After that, the pale green liquid was agitated and alternatively ultrasonically sonicated for 3 h. The obtained white precipitate was collected by centrifugation, thoroughly washed with distillated water, and finally dried at 70 °C overnight. The final product was denoted as PMA@ZIF-8 composite. The synthesis of ZIF-8 was the same as that of PMA@ZIF-8 composite without PMA. The

Table 1 The chemical analysis of the studied ore sample

Component	Wt%	Component	Wt%
SiO_2	25.5	K_2O	0.08
Al_2O_3	0.36	TiO_2	0.01
Fe_2O_3	1.97	P_2O_5	0.02
MgO	15.9	H_2O (110 °C)	0.77
MnO	0.46	LOI (550 °C)	3.83
CaO	22.6	L.O.I* (1000 °C)	28.11
Na_2O	0.05	Total	99.66

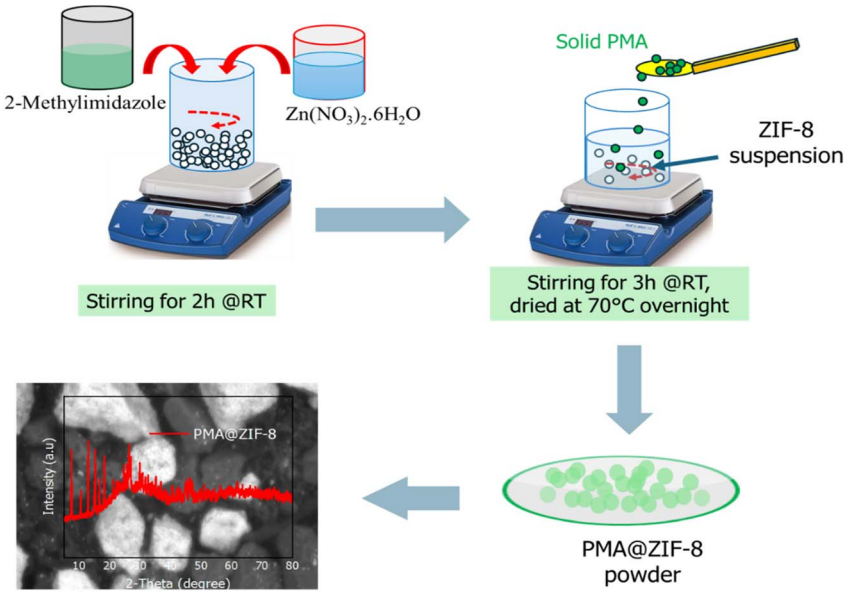

Fig. 1 Steps for the preparation of PMA@ZIF-8 composite at room temperature.

materials obtained were stored in tightly closed bottles for further use without any treatment.

2.4 Characterization

The crystal structure of the prepared samples was obtained using a Bruker D8 advanced X-ray diffractometer with a monochromatized Cu-Kα radiation source ($\lambda = 1.5406$ Å) operated at 40 kV. The functional groups of the synthesized materials were identified using Fourier transform infrared spectroscopy (FTIR). On a Nicolet spectrophotometer (model 6700), the FTIR spectra were obtained using the KBr pellet technique in the 4000–400 cm^{-1} range at a resolution of 2 cm^{-1}. X-ray photoelectron spectroscopy (XPS) measurements were carried out on a VG Multi-Lab 2000 spectrometer to obtain the XPS results of the C, N, O, Zn, and U elements in the prepared PMA@ZIF-8 composites with and without U(VI). A field emission scanning electron microscope (SEM) JSM 7100 F FESEM (Zeiss Ultra Plus) equipped with an energy dispersive spectrum (EDS) analyzer running at 20 kV was used to evaluate the surface morphologies.

2.5 Adsorption study

The adsorption of U(VI) was performed by a batch technique in which all factors affecting the adsorption efficiency, such as solution pH, dosage, contact time, initial U(VI) concentration, and temperature, were examined. Usually, 10 mL of U(VI) solution with an initial concentration of 400 mg L^{-1} was combined with 0.05 g of adsorbent material. The pH of the solutions was adjusted using aqueous solutions of 0.1 M HCl and 0.1 M NaOH. The remaining concentrations of U(VI) were determined by a UV-visible spectrophotometer at a wavelength of 520 nm. In our study, the influence of the initial U(VI) concentration (50–1400 mg L^{-1}), contact time (5–240 min), temperature (25–50 °C), solution pH (8–12), and adsorbent dosage (0.01–0.1 g) on the adsorption process was investigated. The removal percentage (R%) and the adsorption capacity (q_e; mg g^{-1}) of U(VI) were determined by eqn (5) and (6), respectively.

$$R(\%) = \frac{C_0 - C_e}{C_0} \times 100 \quad (5)$$

$$q_e = \frac{(C_0 - C_e)}{M} V \quad (6)$$

where C_0 and C_e are the initial and final U(VI) concentrations (mg L^{-1}), respectively. V is the volume (L), and M is the mass of the adsorbent (g).

Selectivity for U(VI) was evaluated to describe the potency and degree of the selectivity of the prepared adsorbent toward uranium.

3 Results and discussion

3.1 Specifications of alkaline carbonate leach liquors

From the previous works which studied leaching factors of dolostone material collected from SW Sinai, it can be deduced that the optimum conditions for dissolving uranium could be summarized as follows: a grain size of −200 mesh and alkali concentration of Na_2CO_3 (100 g L^{-1}) mixed with $NaHCO_3$ (20 g L^{-1}) in a S/L ratio of 1/3. To the above mixture, 5 mL H_2O_2 was added as the oxidant. Then, the mixture was stirred for 2 h at

Table 2 Chemical composition of the prepared carbonate leach liquor at pH 10 using ICP

Constituent	mg L^{-1}
U	400
REEs	0.5
Cu	0.006
CO^{-2}/HCO^{-}	60

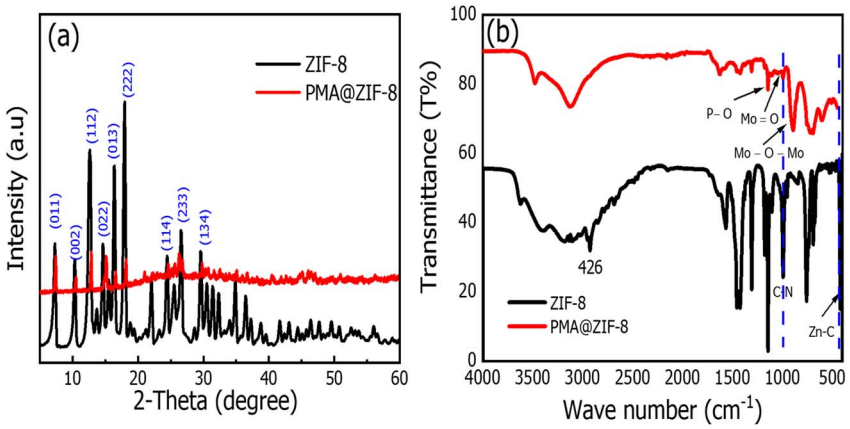

Fig. 2 (a) XRD patterns and (b) FT-IR spectra of ZIF-8 and PMA@ZIF-8.

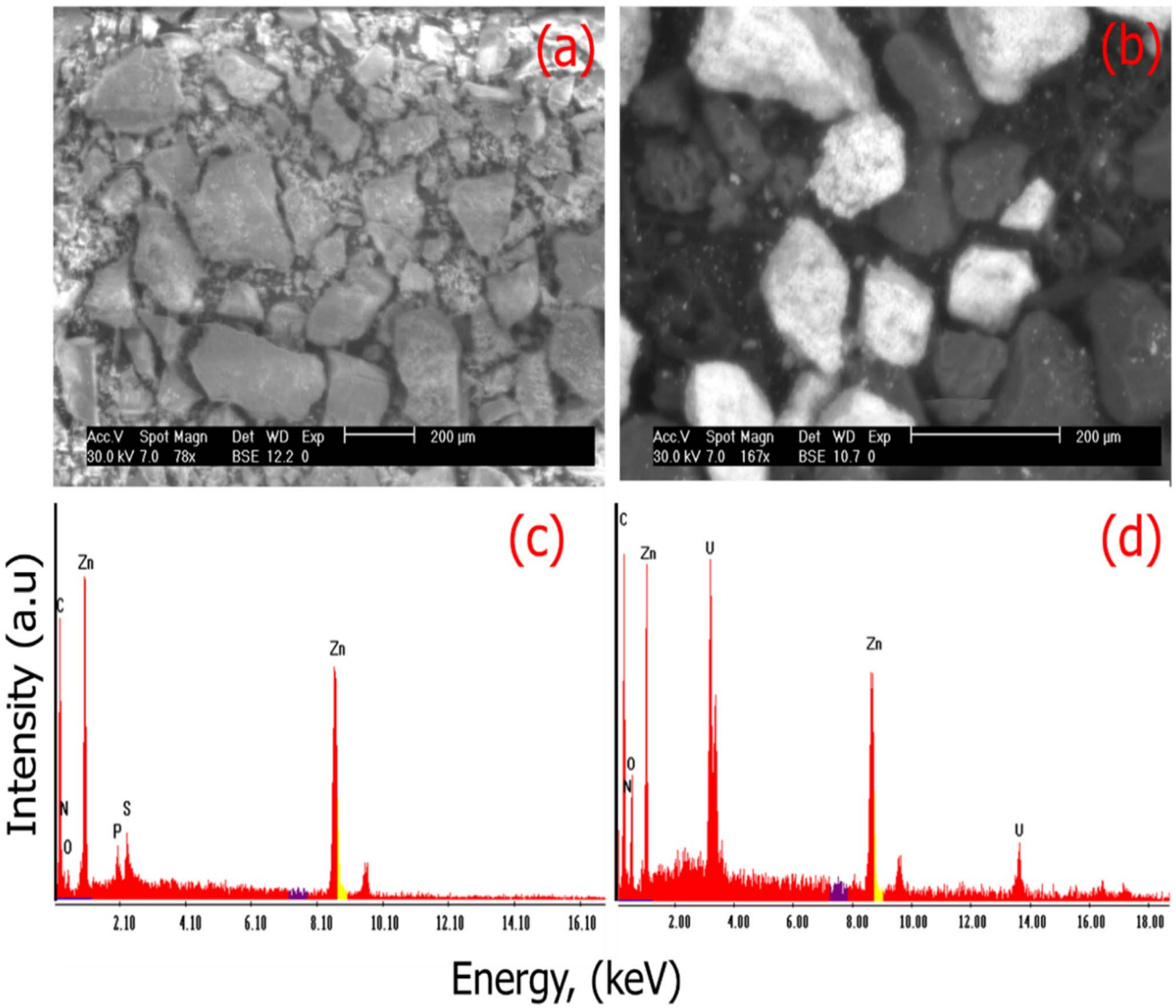

Fig. 3 SEM images of (a) PMA@ZIF-8 and (b) PMA@ZIF-8 loaded with U(VI). EDX analyses of (c) PMA@ZIF-8 and (d) PMA@ZIF-8 loaded with U(VI).

room temperature. Table 2 shows the chemical analysis of the alkaline leach liquor as received by ICP analysis.

3.2 Structural characterization

As described in the experimental procedure, the PMA@ZIF-8 composite was prepared through *in situ* self-assembly of Zn-acetate, 2-MeIM, and PMA. As previously reported, the diameter of PMA is ≈1 nm, which matches well with the cavity size of ZIF-8 (1.1 nm), while being larger than the cage diameter of ZIF-8 (0.34 nm). This is important to prevent the leaching of PMA from the cavities of ZIF-8.[30] More significantly, POMs show substantial Brønsted acidity, which is known to be incompatible with ZIFs in solutions that are susceptible to acid.[30,31]

The crystal structure of the prepared materials was studied by XRD as presented in Fig. 2a. As can be seen, the XRD pattern of the ZIF-8 crystal showed a set of distinctive diffraction peaks at $2\theta = 7.4°$, 10.4°, 12.7°, 14.7°, 16.4°, 18.0°, 22.1°, 24.5°, 26.7°, and 29.6°. These peaks were attributed to the (011), (002), (112), (022), (013), (222), (114), (233), (134), and (044) planes, respectively. These reflections match the sodalite structure (SOD), which is the typical ZIF-8 structure (JCPDS no. 00-062-1030).[29,32,33] On the other hand, the XRD pattern of the PMA@ZIF-8 composite displayed the peaks at the same position as those of ZIF-8, and no peaks for PMA were observed, which is attributed to the encapsulation and high dispersion of PMA in the ZIF-8 cages. Furthermore, the XRD patterns of PMA@ZIF-8 indicate that the encapsulation of PMA causes no damage to the framework structure of ZIF-8.[34] The successful encapsulation of PMA was further verified by FT-IR as presented in Fig. 2b. The distinctive vibration of the Zn–N and C–N bonds, respectively, can be attributed to the peaks at 426 cm^{-1} and 995 cm^{-1} in the FTIR spectra of the ZIF-8 crystal. This further demonstrates that the ZIF-8 crystal was successfully prepared.[30] Additionally, the FT-IR spectra of the PMA@ZIF-8 composite show a number of distinctive peaks at 1065 cm^{-1} (P–O), 995 cm^{-1} (Mo═O), and 890 cm^{-1} (Mo–O–Mo) that are attributed to Keggin units of PMA.[31,35] The PMA@ZIF-8 spectrum demonstrates that the absorption peaks at 426 cm^{-1} and 995 cm^{-1} of ZIF-8 are still detectable, suggesting that ZIF-8 is structurally stable following PMA encapsulation. Additionally, the distinctive stretching vibration peaks of Keggin units are also observed, demonstrating that PMA was successfully encapsulated.

The morphologies and compositions of the PMA@ZIF-8 samples with and without U(VI) ions were characterized by SEM. The surface morphology of the as-prepared PMA@ZIF-8 composite (Fig. 3a) displayed similar morphology except for some spots on the surface of PMA@ZIF-8 loaded with U(VI), as shown in Fig. 3b. This confirms the stability of the PMA@ZIF-8 composite in the adsorption solution. In addition, the energy dispersive X-ray spectroscopy (EDS) analysis of PMA@ZIF-8 (Fig. 3c) displayed the presence of the C, Zn, N, Mo, S, and P

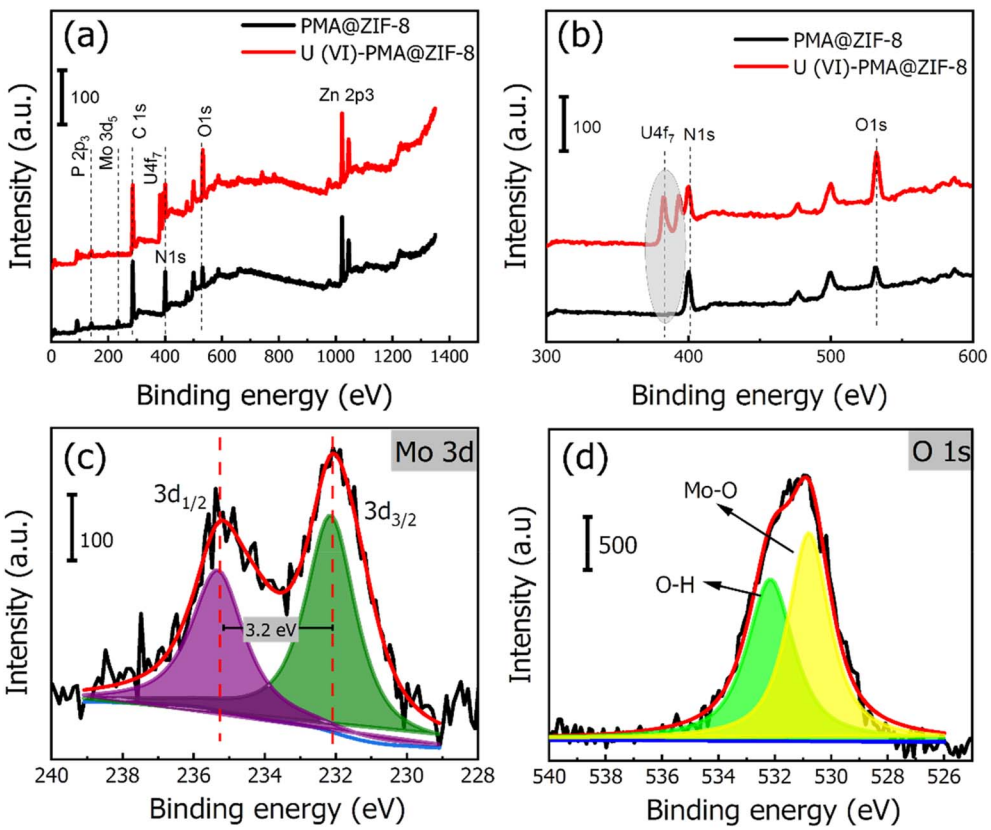

Fig. 4 (a and b) XPS survey of the PMA@ZIF-8 composite after U(VI) adsorption, (c) high-resolution Mo 3d XPS spectrum of the PMA@ZIF-8 composite, and (d) high-resolution O1s XPS spectrum of the PMA@ZIF-8 composite.

elements which also confirms the preparation of the PMA@ZIF-8 composite. On the other hand, the PMA@ZIF-8 loaded with U(VI) in Fig. 3d displays all elements in the pure composite, in addition to the presence of the U element, which confirms the adsorption of U(VI).

To investigate the surface composition and chemical state of PMA@ZIF-8 composites with and without U(VI), the XPS was performed. The XPS survey spectrum of the PMA@ZIF-8 composite (Fig. 4a) indicates the presence of Zn, C, Mo, P, N, O, and C elements. In addition to all these elements, two new split peaks at 392 eV (U $4f_{5/2}$) and 381.05 eV (U $4f_{7/2}$) appeared in PMA@ZIF-8 after adsorbing U(VI) element (Fig. 4b). The XPS survey not only indicates the successful preparation and adsorption process but also confirms the stability of the PMA@ZIF-8 composite in the utilized adsorption media. The high-resolution XPS spectra of Mo 3d in Fig. 4c displayed two peaks at 232.2 and 235.4 eV for Mo $3d_{3/2}$ and Mo $3d_{1/2}$ with a splitting width of 3.2 eV, which coincides with those previously reported.[36] The deconvolution of the XPS spectrum of O1s revealed two peaks at 530.7 and 531.8 eV (Fig. 4d). The peaks correspond to lattice oxygen in Mo–O and to O–H species adsorbed on the oxide surfaces, respectively.[36]

In the high-resolution spectra of C1s (Fig. 5a), the deconvolution reveals a perfect fit with four peaks located at a binding energies of 283.88, 284.58, 285.48, and 288.78 eV, which can be assigned to C–C/C–H, C–O/C–N, C=O, and O=C–OH, respectively.[37] The deconvoluted N 1 s spectrum in Fig. 5b reveals two sub-peaks at ≈398.1 and 401.7 eV, assigned to N atoms in N–C and Mo–N, respectively.[38]

The high-resolution XPS spectrum of P 2p (Fig. 5c) displayed two main peaks at 132.7 and 140.3 eV, assigned to M-P and P–O, respectively. The first peak at 132.7 eV can be fitted into two peaks at 131.7 and 134.2 eV, corresponding to $2P_{3/2}$ and $2P_{1/2}$, respectively.[39] The Zn 2p spectrum (Fig. 5d) includes two peaks at about 1021.6 and 1044.5 eV, assigned to Zn $2p_{3/2}$ and $2p_{1/2}$, respectively. The splitting of 23.1 eV suggests that Zn^{2+} ions

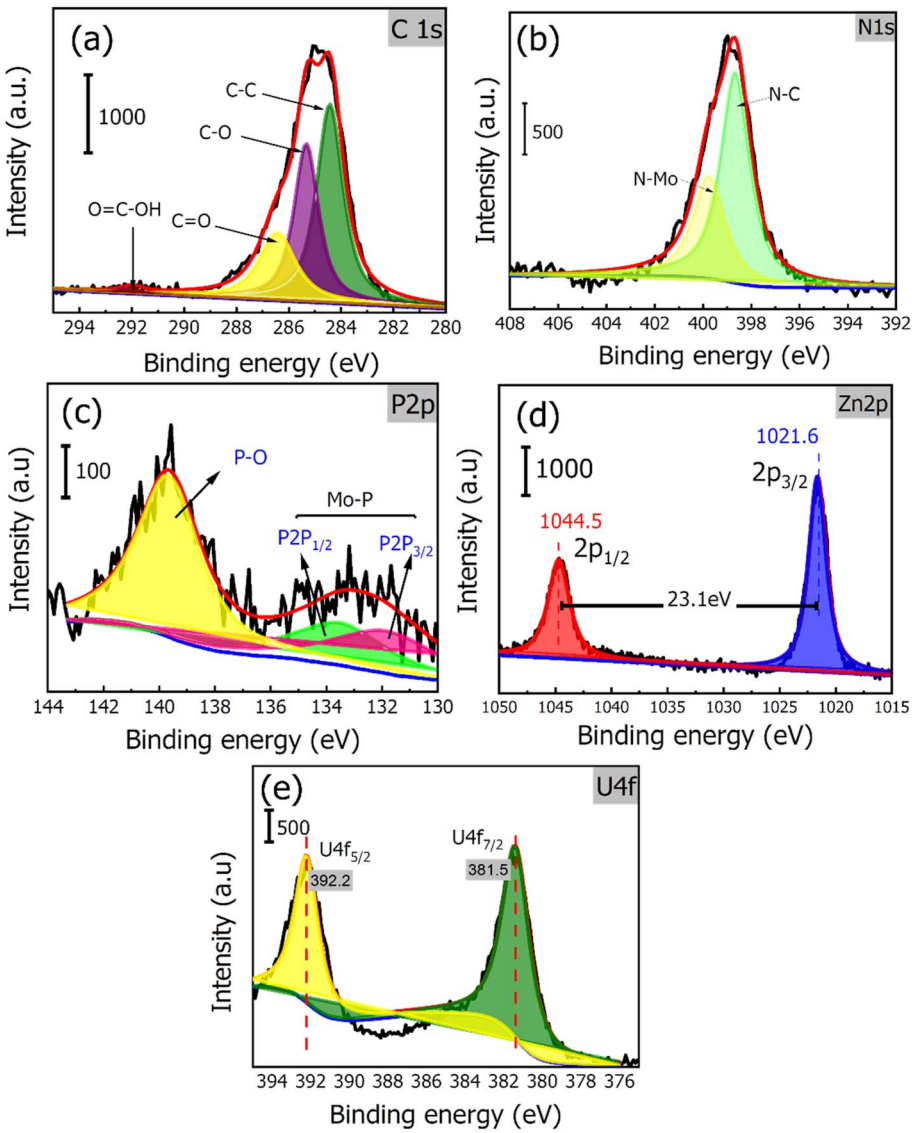

Fig. 5 High-resolution XPS spectra of (a) C1s, (b) N1s, (c) P2p, (d) Zn2p, and (e) U(VI) of the PMA@ZIF-8 composite.

exist in the composite due to the formation of ZIF-8.[40] The high-resolution spectra of U 4f in Fig. 5e showed two peaks around 392.2 eV (U $4f_{5/2}$) and 381.5 eV (U $4f_{7/2}$), confirming the adsorption of U(VI).[41]

4 Adsorption studies

4.1 Adsorption capacity

The adsorption capacity was evaluated by stirring 0.01 g of the PMA@ZIF-8 composite with 10 mL of U(VI) with initial concentrations ranging from 50 mg L^{-1} to 400 mg L^{-1}. After adjusting the pH of the U(VI) solutions to 10.5, the mixtures were agitated for 90 minutes at 25 °C. As presented in Fig. 6a, the adsorption capacity of the PMA@ZIF-8 composite was gradually enhanced with increasing the initial U(VI) concentration from 50 mg L^{-1} to 1200 mg L^{-1}, followed by a slight increase, and finally a barely noticeable increase at 1400 mg L^{-1}. The adsorption capacity was increased from 49 to 124 mg g^{-1} by increasing the initial concentration of U(VI) from 50 to 1200 mg L^{-1}, respectively. With further increases in the initial concentration from 1200 to 1400 mg L^{-1}, no remarkable enhancement in the adsorption capacity was observed. The maximum uptake of U(VI) onto the PMA@ZIF-8 composite was 124 mg g^{-1}. The increase in U(VI) uptake with increasing initial U(VI) concentration is mainly attributed to the enhancement of the mass transfer driving force *via* several collisions between U(VI) molecules and the surface of the adsorbent.[42]

4.2 Effect of pH

The adsorption is usually influenced by the pH, as it determines the ionization of the adsorbate and the charge of the adsorbent surface. Additionally, changing the pH values plays a critical role in protonating and deprotonating the functional groups on adsorbents and adsorbate molecules, thereby enhancing their electrostatic interactions.[43] Thus, the effect of pH on the adsorption of U(VI) onto the PMA@ZIF-8 composite was tested by varying pH values over the range of 8–12. In each experiment, U(VI) solutions with initial concentration of 400 mg L^{-1} were mixed with 0.05 g of adsorbent, and the mixtures were kept under shaking for 60 min at 25 °C. As shown in Fig. 6b, the removal efficiency of U(VI) was significantly enhanced from 17.31% to 80.77% by increasing pH from 8 to 10.5. Upon further increasing the pH to 12, the removal efficiency was reduced to 10.0%. Furthermore, it was also observed that the U(VI) uptake by PMA@ZIF-8 composite was gradually increased from 12 to 60 mg g^{-1} by increasing pH from 8 to 10.5, respectively. At a pH of 12, however, the uptake was reduced to 8 mg g^{-1}. This was mainly attributed to the fact that the adsorption of U(VI) molecules onto the PMA@ZIF-8 composite was driven by the electrostatic attraction between the adsorbed H^+ groups and the U(VI) ions. Under the strong alkaline conditions, the high competition between adsorption sites on the surface of the adsorbent caused by excess OH^- ions and the U(VI) on the available adsorption sites led to decreased adsorption.[44]

The influence of pH on U(VI) ion sorption can be interpreted in terms of both the surface properties of the adsorbents and the speciation of uranium in solution. The adsorption–pH profiles were generated and presented in Fig. 7. The effect of pH on U(VI) adsorption may be understood on the basis of uranium speciation in solution and the surface charge of the adsorbent. As shown in Fig. 7, in acidic pH (≤3), U(VI) exists as free uranyl ions (UO_2^{2+}) with high electrostatic attraction to negatively charged surface functional groups of the adsorbent and

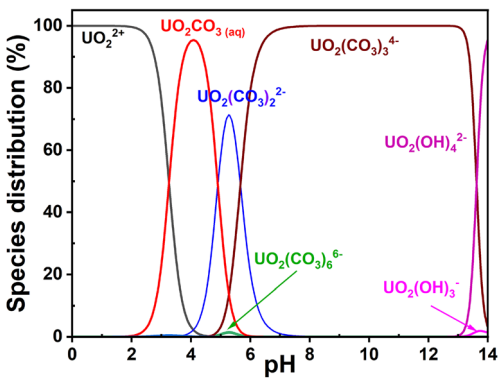

Fig. 7 The distribution of U(VI) species as a function of pH in the aqueous solution (400 mg L^{-1} (0.0016804 M) uranium ions, 80 g L^{-1} carbonate + 20 g bicarbonate).

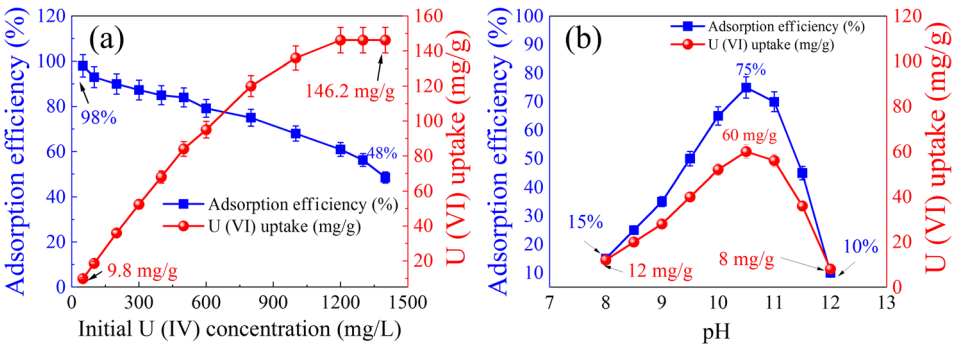

Fig. 6 Effect of (a) initial concentration and (b) solution pH on the removal percentage and U(VI) uptake by the PMA@ZIF-8 composite from alkaline aqueous solution.

therefore exhibits high adsorption efficiency. At the near-neutral pH (pH 4–8) range, the complexation of carbonate becomes significant, and species such as UO_2CO_3(aq), $UO_2(CO_3)_2^{2-}$, and $UO_2(CO_3)_3^{4-}$ are produced. These anionic complexes have weaker affinity for negatively charged adsorbent surfaces, thereby reducing sorption efficiency. At alkaline pH (>10), hydrolyzed species such as $UO_2(OH)_3^-$ and $UO_2(OH)_4^{2-}$ dominate, and the strong competition with hydroxyl and carbonate ions further limits adsorption. These results indicate that uranium uptake is strongly regulated by the pH-dependent speciation of U(VI).

4.3 Effect of contact time

One of the most important factors in controlling the overall adsorption process is the contact time between adsorbent and adsorbate. Therefore, using U(VI) solutions with an initial concentration of 400 mg L^{-1} and acidity adjusted to a pH of 10.5, the impact of contact duration on the removal efficiency of U(VI) by the PMA@ZIF-8 composite was examined. In each experiment, 10 mL of U(VI) solution was mixed with 0.05 g of adsorbent and shaken for various times (5–240 min) at 25 °C. As shown in Fig. 8a, the removal of U(VI) increased from 2.5 to 81.25% by increasing the time from 5 to 90 min, respectively. Further increase in time to 240 min led to no significant enhancement in the removal efficiency. Higher adsorption at the early stage (*i.e.*, until 90 min) can be assigned to the presence of more unoccupied adsorption sites. In the later stage, an adsorption plateau was observed due to the interactions between the U(VI) molecules on the adsorbent and the bulk phase becoming more and more repulsive.[45] Moreover, the maximum U(VI) uptake was 88 mg g^{-1} at 90 min.

4.4 Effect of adsorbent dosage

The adsorbent dosage is an essential factor in avoiding the waste of the adsorbent material after reaching equilibrium.[46] The effect of the adsorbent on the adsorption of U(VI) was studied by varying the dosage of the PMA@ZIF-8 composite from 1 to 10 g L^{-1}. The pH was adjusted to 10.5, followed by shaking for 90 min at 25 °C. As shown in Fig. 8b, by increasing the weight of the PMA@ZIF-8 composite from 1 to 10 g, the removal of U(VI) gradually increased, which could be attributed to the greater number of active sites available for interaction with U(VI) ions.

4.5 Adsorption kinetics

To examine the kinetic behavior of U(VI) adsorption by the PMA@ZIF-8 composite, the experimental data were tested using two kinetic models, namely, the pseudo-first-order and pseudo-second-order models, at different temperatures. The pseudo-first-order model is expressed by eqn (7).[47,48]

$$\ln(q_e - q_t) = \ln q_e - k_1 t \quad (7)$$

The pseudo-second-order equation is expressed by eqn (8).[49]

$$\frac{t}{q_t} = \frac{1}{k_2 q_e^2} + \frac{t}{q_e} \quad (8)$$

where q_e (mg g^{-1}) and q_t (mg g^{-1}) are the amount of the U(VI) adsorbed at equilibrium and time t, respectively. k_1 (min^{-1}) and k_2 (g mg^{-1} min^{-1}) are the rate constants of the pseudo-first-order and pseudo-second-order kinetic models, respectively.

The fitted linear kinetic models for the adsorption of U(VI) are presented in Fig. 9a and b, and their estimated kinetic parameters are listed in Table 3. It can be observed that the experimental data of U(VI) adsorption onto the PMA@ZIF-8 composite are best fitted with the pseudo-second-order kinetic model, as indicated by the higher correlation coefficient (R^2) values. Therefore, the adsorption of U(VI) by the PMA@ZIF-8 composite is a chemisorption process.[50] The estimated q_e values from the pseudo-second-order models for the adsorption of U(VI) onto the PMA@ZIF-8 composite are 93.54, 51.55, 30.12, and 17.04 mg g^{-1} at 25, 30, 40, and 50 °C, respectively. The decrease in U(VI) uptake with increasing temperature indicates an exothermic process.

4.6 Adsorption isotherms

The adsorption isotherm is necessary to convey the adsorption capacity and to describe the interaction between the adsorbent and the adsorbate molecules. Adsorption equilibrium is regarded as a dynamic notion in the description of adsorption isotherms, demonstrating that the rate of dye adsorption is

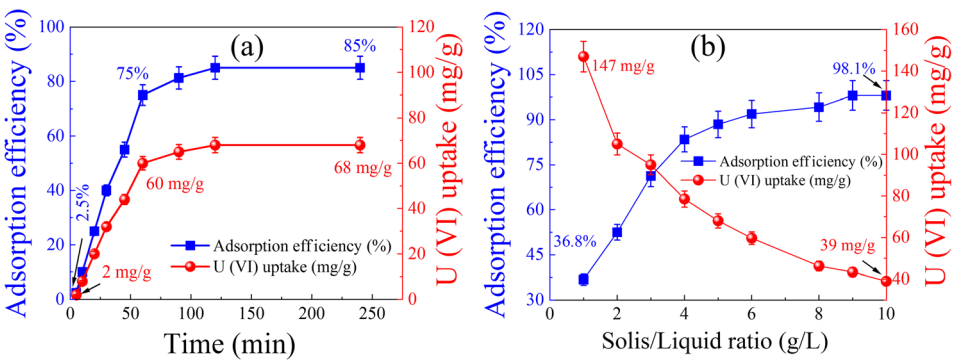

Fig. 8 Effect of (a) contact time and (b) adsorbent dose on the removal percentage and U(VI) uptake from alkaline leach liquor by the PMA@ZIF-8 composite.

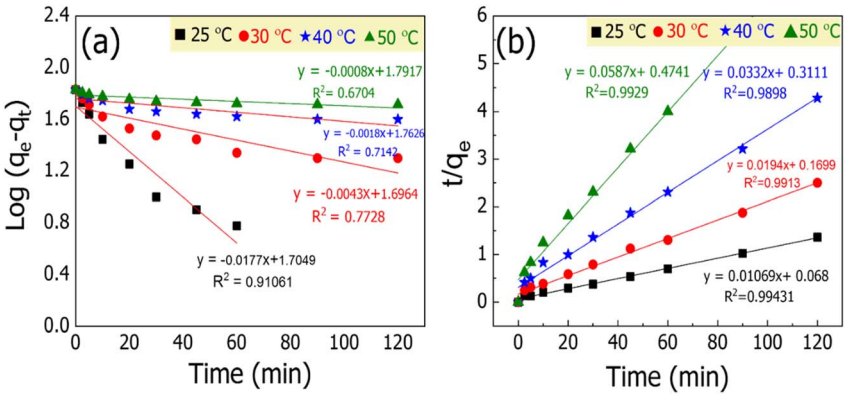

Fig. 9 Experimental and linear kinetic models for the adsorption of U(VI) onto the PMA@ZIF-8 composite: (a) pseudo-first-order and (b) pseudo-second-order models.

Table 3 The kinetic parameters estimated from linear kinetic models for the adsorption of U(VI) onto the PMA@ZIF-8 composite

Kinetic model	Parameter	25 °C	30 °C	40 °C	50 °C
Pseudo-first order	q_e (mg g^{-1})	5.500	5.454	5.827	5.999
	k_1 (min^{-1})	−0.018	−0.004	−0.002	−0.001
	R^2	0.911	0.773	0.714	0.670
Pseudo-second order	q_e (mg g^{-1})	93.540	51.550	30.120	17.040
	k_2 (g mg^{-1} min^{-1})	0.0017	0.0022	0.0004	0.0073
	R^2	0.994	0.991	0.998	0.993

equal to the rate of dye desorption. This equilibrium test thus provides physio-chemical evidence for the adsorption method's viability. Typically, the surface of the adsorbent can be categorized as either monolayer or multilayer. The Langmuir and Freundlich isotherm models are frequently used to describe solid–liquid adsorption systems. A monolayer adsorption onto a uniform surface with a finite number of identical sites is described by the Langmuir model. The linear form of the Langmuir model is represented by eqn (9).[51]

$$\frac{C_e}{q_e} = \frac{1}{(q_{max} \times b)} + \frac{1}{q_{max} \times C_e} \quad (9)$$

Multilayer adsorption systems and heterogeneous surfaces are explained by the Freundlich model, whose linear version is provided by eqn (10):[52]

$$\mathrm{Ln}q_e = \mathrm{Ln}K_f + \left(\frac{1}{n_f}\right)\ln\ C_e \quad (10)$$

where q_{max} (mg g^{-1}) is the maximum adsorbate capacity, K_L (L mg^{-1}) is the Langmuir constant, b is the Langmuir constant, and K_f and n_f are the Freundlich constants.

As presented in the isotherm plots in Fig. 10 and their related parameters in Table 4, it can be observed that the adsorption of U(VI) onto the PMA@ZIF-8 composite obeyed the Langmuir isotherm model with a higher correlation coefficient (R^2 =

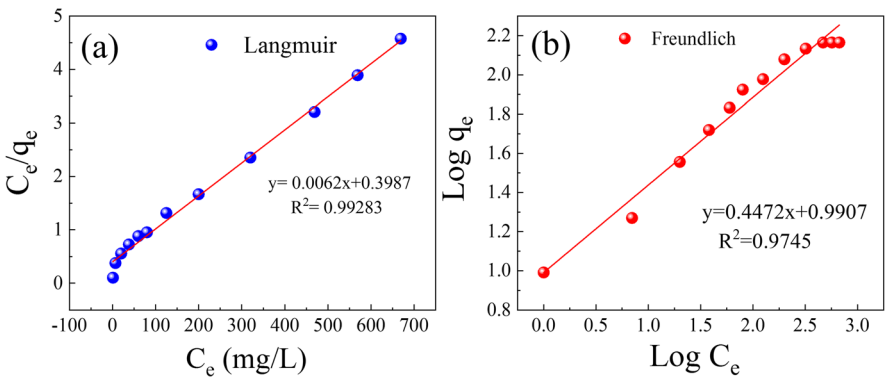

Fig. 10 The experimental data and linear isotherm models for the adsorption of U(VI) ions onto the PMA@ZIF-8 composite: (a) Langmuir and (b) Freundlich isotherm models.

Table 4 Adsorption isotherm parameters for U(VI) adsorption onto the PMA@ZIF-8 composite

	Langmuir			Freundlich		
	q_{max} (mg g^{-1})	b (L mg^{-1})	R^2	K_f (mg g^{-1}) (L mg^{-1})$^{1/n}$	n_f	R^2
PMA@ZIF-8	161.29	15.55×10^{-3}	0.993	2.693	2.236	0.974

0.993) than that of the Freundlich isotherm model ($R^2 = 0.974$). This indicates the formation of a U(VI) monolayer on the surface of the PMA@ZIF-8 composite.[53] The interaction between an adsorbate and an absorbent is typically described by the Langmuir constant b. The value of b for U(VI) is 15.55×10^{-3} L mg^{-1}. The estimated maximum adsorption capacity of U(VI) ions was 161.29 mg g^{-1}, and such an adsorption capacity is mainly due to the higher surface area and the presence of PMA molecules, which act as active centers for adsorption.

Table 5 Thermodynamic parameters for the adsorption of U(VI) onto the PMA@ZIF-8 composite

Parameters	$\Delta H°$ (kJ mol^{-1})	$\Delta S°$ (J mol^{-1} K^{-1})	
Values	−26.17	−80.38	
$\Delta G°$ (kJ mol^{-1})			
25 °C	30 °C	40 °C	50 °C
23.93	24.33	25.13	25.94

4.7 Effect of temperature

The effect of temperature on the ability of the PMA@ZIF-8 composite to adsorb U(VI) ions was investigated at four different temperatures: 25, 30, 40, and 50 °C. In each experiment, 10 mL of U(VI) with an initial concentration of 400 mg L^{-1} and pH 10.5 was mixed with 0.05 g of adsorbent and shaken for 90 minutes at the desired temperature values. As presented in Fig. 11a, the removal efficiency of U(VI) is reduced by increasing the temperature from 25 to 50 °C, which indicates that the adsorption mechanism is exothermic.[54] This is typically due to the removal of U(VI) through adsorption being an exothermic process, whereby removal is thermodynamically favorable at lower temperatures. At elevated temperatures, binding capacity and adsorption capability decrease, leading to reduced efficiency.[55] Thus, 25 °C (298 K) might be considered the ideal temperature for U(VI) adsorption tests, which agrees with the previous reports.[55,56] The various thermodynamic parameters, including the change in Gibbs free energy (ΔG^o), enthalpy (ΔH^o), and entropy (ΔS°), were estimated by van't Hoff plots.[54] These parameters were used to explore the nature of the adsorption process as exothermic or endothermic, as well as the degree of the disorder (eqn (11)–(13)).

$$\ln K_d = \frac{\Delta S^\circ}{R} - \frac{\Delta H^\circ}{RT} \quad (11)$$

$$\Delta G^\circ = \Delta H^\circ - T\Delta S^\circ \quad (12)$$

$$\Delta G^\circ = -RT \ln K_d \quad (13)$$

where $\Delta S°$ (J mol^{-1} K^{-1}), $\Delta G°$ (kJ mol^{-1}), and $\Delta H°$ (kJ mol^{-1}) represent the changes in entropy, Gibbs free energy, and enthalpy, respectively. T is the adsorption temperature (Kelvin), R is the gas constant (8.3145 J mol^{-1} K^{-1}), and K_d (Q_e/C_e) is the distribution coefficient.

The numerical values of $\Delta H°$, $\Delta S°$, and $\Delta G°$ were estimated from the slope and intercept of the Van't Hoff plots of ln K_d *vs.* 1/T (Fig. 11b). The estimated values of $\Delta H°$, $\Delta S°$, and $\Delta G°$ are listed in Table 5. The positive values of $\Delta G°$ indicate that adsorption is not spontaneous and is thermodynamically unfavorable, which confirms the kinetic analysis discussed above.[57] In contrast, the negative value of $\Delta S°$ indicates a decrease in randomness and disorder at the liquid–solid interface during the adsorption.[58] The negative value of $\Delta H°$ denotes the exothermic nature of the adsorption process. This

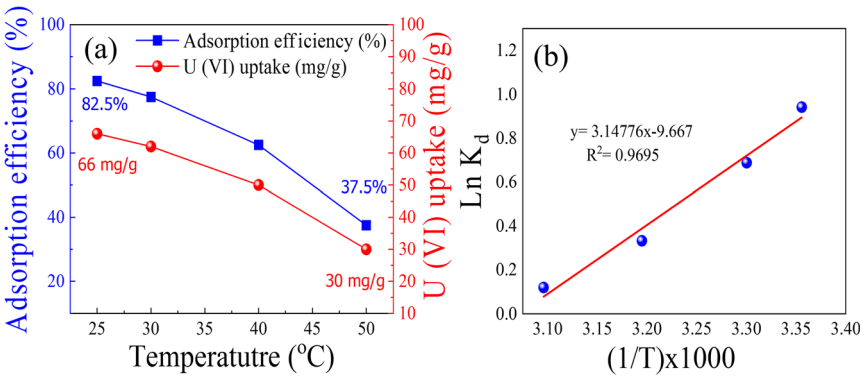

Fig. 11 (a) Effect of temperature and (b) van't Hoff plot for the adsorption of U(VI) ions by the PMA@ZIF-8 composite.

suggests that an increase in temperature is not favorable for the adsorption performance.

4.8 Selective adsorption

The PMA@ZIF-8 composite selectivity for the adsorption of U(VI) over various metal ions found in wastewater was evaluated using a mixed-ion solution consisting of U, La, Zn, Ni, Y, Zr, Fe, V, Ti, Pb, Cd, Cu, and Mn. The PMA@ZIF-8 composite exhibited a far higher adsorption affinity for U(VI) compared to other metal ions, as shown in Fig. 12. The adsorption efficiency for uranyl ions was 84.5%, that is, a figure approximately 81–97% higher than the adsorption efficiencies for the other elements under test. The results verify the great selectivity of the composite for uranium and present evidence of its significant potential for industrial-scale uranium removal processes. The selectivity of PMA@ZIF-8 for U(VI) is great because of many synergistic factors. Initially, the PMA has rich oxygen-containing functional groups, *e.g.*, P–O and Mo=O, that are good hard coordination sites for the uranyl ion (UO_2^{2+}), whose geometry is linear and hard Lewis base donor affinity is strong. Secondly, the uranyl ion is known to have a high chelating affinity for polydentate ligands, and the structure of PMA is highly favorable for coordination due to its Keggin-type framework. Additionally, the porosity of ZIF-8 has large surface area and accessible pore channels that allow for easy diffusion and contact of U(VI) with active sites. The size-exclusion effect of ZIF-8 may also play a role to a smaller degree by excluding competitive metal ions with larger hydrated radii or incompatible coordination needs. Generally, these contributions result in the enhanced and selective adsorption of the U(VI) ion from more complex aqueous solutions.[59,60]

4.9 Desorption experiments

Recovery or desorption of uranium loaded on the PMA@ZIF-8 composite was investigated using some eluates including HCl, H_2SO_4, HNO_3, NaOH, Na_2CO_3, NaCl, Na_2SO_4, and CH_3COONa. In our work, desorption experiments were performed by mixing 0.1 g of the PMA@ZIF-8 composite loaded with uranium with 10 mL of the eluent solution (1.0 M), followed by shaking for 60 min. The overall desorption efficiency was calculated and listed in Table 6. It can be observed that diluted HNO_3 is the best eluent, as indicated by achieving more than 94.9% recovery of uranium from the adsorbent in a single contact method.

Table 6 Uranium recovery from the loaded PMA@ZIF-8 composite using different solutions

Eluent type (1.0 M)	Efficiency (%)
H_2SO_4	85.3
HCl	83.4
HNO_3	94.9
NaCl	69.1
CH_3COONa	25.4
Na_2SO_4	35.9
Na_2CO_3	76.5
NaOH	84.8

Table 7 Adsorption and desorption cycles for uranium recovery using the PMA@ZIF-8 composite

No. of cycle	Sorption efficiency (%)	Desorption efficiency (%)
1	96.3	90.1
2	89.4	83.2
3	76.4	68.6
4	68.7	56.3
5	52.2	41.5
6	47.4	34.9
7	32.8	22.7

4.10 Reusability

The most significant aspect of the practical use of adsorbents is reusability. Because of the reversible adsorption process, the adsorbent may be regenerated, which is necessary for both economic viability and resourcefulness. Consequently, cyclic

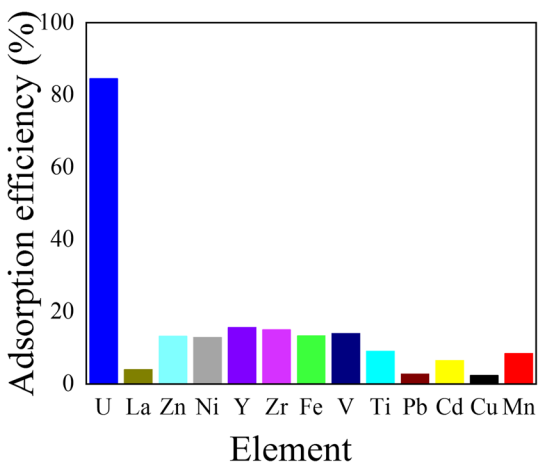

Fig. 12 Effect of competitive ions on the adsorption of U(VI) onto the PMA@ZIF-8 composite.

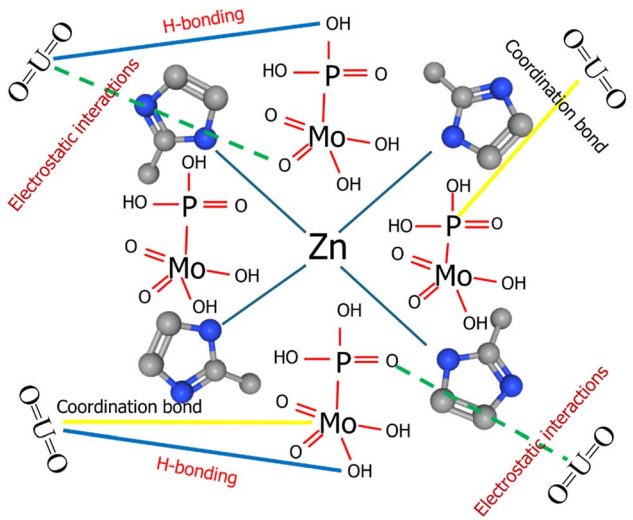

Fig. 13 Possible adsorption mechanism of uranium (VI) onto the PMA@ZIF-8 composite.

Table 8 Comparison of U(VI) adsorption capacity of different adsorbents

Adsorbent material	Conditions (pH/medium)	Q_{max} (mg g^{-1})	Ref.
Activated carbon (Al-modified)	Neutral	24.5	63
Calcium-phosphate modified activated carbon	Neutral	58	63
Corn-cob powder	pH ~5	7–14	64
Lysinibacillus-GO	Neutral–Slightly acidic	149.3	65
Chitosan/ZIF-8 composite	Acidic (pH 3)	629	26
Phosphomolybdic acid@ZIF-8	**Alkaline, pH 10.5**	**124**	This work

absorption–desorption tests were conducted to examine the reusability of the PMA@ZIF-8 composite.

Table 7 shows that the PMA@ZIF-8 composite's adsorption efficiency decreased somewhat with each recycling cycle, but remained high even after seven cycles of repeated use. The results proved the potential of the PMA@ZIF-8 composite adsorbent for uranium adsorption from the carbonate solutions.

4.11 Adsorption mechanism

SEM-EDX analysis of the U(VI)-loaded composite PMA@ZIF-8 (Fig. 3b) confirms the adsorption of U(VI) to be effective, based on the presence of the uranium peaks along with the compositional elements characteristic of the composite (C, Zn, N, Mo, S, and P). The presence of these signals even after adsorption suggests the stability of the PMA@ZIF structure at alkaline pH. To better understand the mechanism of interaction, XPS spectra of PMA@ZIF-8 before and after adsorption of U(VI) were investigated (Fig. 4a and b). Two distinct peaks at binding energies of 392.0 eV (U $4f_{5/2}$) and 381.5 eV (U $4f_{7/2}$) were found after adsorption, confirming the immobilization of U(VI) species on the composite surface.[41,61] Shifts in the O 1s and Mo 3d region (not included herein) signify coordination of uranyl ions with oxygen atoms in PMA, demonstrating the role of Mo–O and P–O groups as active binding sites. The pseudo-second-order model described the adsorption kinetics best, indicating chemisorption-controlled adsorption.[50] The Langmuir isotherm model also best described the data at equilibrium, suggesting monolayer coverage of U(VI) ions at the composite surface.[53]

Mechanistically, several types of interactions are involved: (i) electrostatic interaction between positively charged U(VI) species and negatively charged oxygen atoms of PMA; (ii) coordination bonding of uranyl ions with donor atoms (O, Mo, P) in PMA; (iii) hydrogen bonding between PMA hydroxyl groups and uranyl species; and (iv) the porous natutre of ZIF-8 framework, provides a high surface area and pore channels that enhance the dispersion and accessibility of the PMA active sites.[62]

Overall, the U(VI) adsorption onto PMA@ZIF-8 is a coordination bonding-, electrostatic interaction- and hydrogen bonding-induced chemisorption process.[30] Fig. 13 presents the proposed adsorption mechanism.

4.12 Comparison of U(VI) adsorption capacity of different adsorbents

Table 8 provides the U(VI) adsorption capacity of different adsorbents under different pH conditions. Most of the reported adsorbents, such as biomass-derived and activated carbon, possess low adsorption capacity under near-neutral or weakly acidic medium. Despite having an extremely high capacity (629 mg g^{-1}), chitosan/ZIF-8's activity is only accessible under strongly acidic medium (pH 3). Compared to this, phosphomolybdic acid@ZIF-8 synthesized herein realizes a high adsorption capacity of 124 mg g^{-1} at alkaline pH 10.5. Such high performance is of particular significance since U(VI) generally exists as stable uranyl–carbonate complexes under alkaline conditions, which are generally difficult to capture. Therefore, the present material evidently has distinct advantages in the treatment of alkaline uranium-containing wastewater, where general adsorbents are less effective.

5 Conclusions

In this study, a PMA@ZIF-8 composite was prepared *via* a simple *in situ* process to be utilized for removal of U(VI) from the alkaline leach liquor of dolostone ore material. The prepared composite displayed promising ability toward adsorption of U(VI), and the maximum adsorption capacity was 124 mg g^{-1} after 90 min at pH 10.5. The isotherm analysis confirms that the experimental data of adsorption of U(VI) onto the PMA@ZIF-8 composite obeyed the Langmuir model, with an estimated adsorption capacity of 132.6 mg g^{-1}. Additionally, the kinetic study confirmed that the adsorption of U(VI) obeyed the pseudo-second-order kinetic model. The thermodynamic study showed that the adsorption process is exothermic in nature and thermodynamically unfavorable. These findings demonstrate the PMA@ZIF-8 composite is highly effective for the recovery of U(VI) ions from the alkaline media at room temperature.

Conflicts of interest

There are no conflicts to declare.

Data availability

All relevant data to support this research are given in the article.

References

1 T. Sreenivas and J. K. Chakravartty, Alkaline processing of uranium ores of indian origin, *Trans. Indian Inst. Met.*, 2016, **69**(1), 3.

2 L. Li, N. Hu, D. Ding, X. Xin, Y. Wang, J. Xue, H. Zhang and Y. Tan, Adsorption and recovery of U(VI) from low concentration uranium solution by amidoxime modified Aspergillus niger, *RSC Adv.*, 2015, **5**(81), 65827.

3 A. Nighojkar, R. S. Kothale and B. Kandasubramanian, Functionalized polymeric architectures (FPAs) for uranium recovery from oceans: A review on adsorptive approaches, models and spectrophotometry for understanding the interaction mechanism, *J. Hazard. Mater. Adv.*, 2023, **9**, 100210.

4 I. W. Mwangi and J. C. Ngila, Removal of heavy metals from contaminated water using ethylenediamine-modified green seaweed (Caulerpa serrulata), *Phys. Chem. Earth, Parts A/B/C*, 2012, **50–52**, 111.

5 Z. Sun, Z. Chen, X. Tai and X. Wang, Uranium extraction from seawater: methods and challenges, *Sci. China:Chem.*, 2025, **68**(9), 3923.

6 R. M. Attia, Extraction of uranium and copper from acid leached solid waste of Alluoga sedimentary rocks, Southwestern Sinai, Egypt, *J. Radioanal. Nucl. Chem.*, 2022, **331**(10), 4297.

7 A. L. El-Ansary, G. M. Abd El-Wahab, E. E. Bayoumi and E.-S. A. Nouh, Purification of Abu-Zenima wet crude yellow cake using alkaline leaching of U(VI), *Egypt. J. Pet.*, 2018, **27**(4), 523.

8 S. Abdel Wahab, A. Rezik, H. A. Abu Khoziem, E. Khalid and W. Abdellah, Kinetics of uranium carbonate leaching process from carbonaceous shale, southwestern Sinai, Egypt, *Euro-Mediterr. J. Environ. Integr.*, 2019, **4**(1), 19.

9 C. Zhou, A. Ontiveros-Valencia, L. Cornette de Saint Cyr, A. S. Zevin, S. E. Carey, R. Krajmalnik-Brown and B. E. Rittmann, Uranium removal and microbial community in a H_2-based membrane biofilm reactor, *Water Res.*, 2014, **64**, 255.

10 E. L. S. A. Haggag, Cellulose hydrogel for enhanced uranium (VI) capture from nitrate medium: preparation, characterisation and adsorption optimisation, *Int. J. Environ. Anal. Chem.*, 2023, **103**(20), 9250.

11 M. A. Embaby, E.-s. A. Haggag, A. S. El-Sheikh and D. A. Marrez, Biosorption of Uranium from aqueous solution by green microalga Chlorella sorokiniana, *Environ. Sci. Pollut. Res.*, 2022, **29**(38), 58388.

12 D. Pyle, H. Blatt and R. J. Tracy, 1996. Petrology. Igneous, Sedimentary, and Metamorphic, 2nd ed., New York, Basingstoke, W. H. Freeman, *Geol. Mag.*, 1997, (1), 121.

13 J. Warren, Dolomite: occurrence, evolution and economically important associations, *Earth-Sci. Rev.*, 2000, **52**(1), 1.

14 X. T. Chen, L. F. He, R. Z. Liu, C. Zhang, B. Liu and Y. P. Tang, Effective uranium(VI) sorption from alkaline media using bi-functionalized silica-coated magnetic nanoparticles, *RSC Adv.*, 2015, **5**(70), 56658.

15 L.-Y. Yuan, Y.-L. Liu, W.-Q. Shi, Y.-L. Lv, J.-H. Lan, Y.-L. Zhao and Z.-F. Chai, High performance of phosphonate-functionalized mesoporous silica for U(vi) sorption from aqueous solution, *Dalton Trans.*, 2011, **40**(28), 7446.

16 S. Fortier and T. W. Hayton, Oxo ligand functionalization in the uranyl ion (UO22+), *Coord. Chem. Rev.*, 2010, **254**(3), 197.

17 D. L. Clark, S. D. Conradson, R. J. Donohoe, D. W. Keogh, D. E. Morris, P. D. Palmer, R. D. Rogers and C. D. Tait, Chemical speciation of the uranyl ion under highly alkaline conditions. synthesis, structures, and oxo ligand exchange dynamics, *Inorg. Chem.*, 1999, **38**(7), 1456.

18 P. Zong, S. Wang, Y. Zhao, H. Wang, H. Pan and C. He, Synthesis and application of magnetic graphene/iron oxides composite for the removal of U(VI) from aqueous solutions, *Chem. Eng. J.*, 2013, **220**, 45.

19 Y. Xie, L. Yu, L. Chen, C. Chen, L. Wang, F. Liu, Y. Liao, P. Zhang, T. Chen, Y. Yuan, *et al.*, Recent progress of radionuclides separation by porous materials, *Sci. China:Chem.*, 2024, **67**(11), 3515.

20 D. Tolan, A. El-Sawaf, A. S. A. Ahmed, A. Nassar, N. M. Mohamed, I. G. Alhindawy, E. A. Elshehy and V. Utgikar, Enhanced photocatalytic activity of (In–Sr–P) tridoped TiO_2/Bi_2O_3 composite loaded on mesoporous carbon: A facile sol-hydrothermal synthesis approach, *Mater. Chem. Phys.*, 2024, **322**, 129570.

21 A. El-Sawaf, D. A. Tolan, M. S. Abdelrahman, I. A. El-Hay, M. Ismael, A. S. A. Ahmed, E. A. Elshehy and M. T. Abdu, Fast in-situ synthesis of mesoporous Prussian blue-silica nanocomposite for superior silver ions recovery performance, *J. Chem. Technol. Biotechnol.*, 2024, **99**(9), 1941.

22 S. R. A. Younis, M. Abdelmotallieb and A. S. A. Ahmed, Facile synthesis of ZIF-8@GO composites for enhanced adsorption of cationic and anionic dyes from their aqueous solutions, *RSC Adv.*, 2025, **15**(11), 8594.

23 K. Patra, S. Mollick, A. Sengupta and S. R. Guchhait, Unlocking a radioactive pertechnetate (TcO_4^-) treatment process with functionalized metal–organic frameworks (MOFs), *Nanoscale Adv.*, 2025, **7**(4), 984.

24 H. Lu, D. Fu, X. Tai, Z. Sun and X. Wang, Metal–organic frameworks/covalent–organic frameworks-based materials in organic/inorganic pollutant elimination and CO_2 reduction applications, *ChemNanoMat*, 2025, 2500244.

25 K. Tuo, J. Li, Y. Li, C. Liang, C. Shao, W. Hou, Z. Li, S. Pu and C. Deng, Construction of hierarchical porous and polydopamine/salicylaldoxime functionalized zeolitic imidazolate framework-8 *via* controlled etching for uranium adsorption, *Mater. Horiz.*, 2024, **11**(14), 3364.

26 L. Liu, W. Yang, D. Gu, X. Zhao and Q. Pan, In situ preparation of chitosan/ZIF-8 composite beads for highly efficient removal of U(VI), *Front. Chem.*, 2019, 7.

27 D. Liu, Y. Wang, L. Zuo, M. Guo and S. Liu, Advanced materials for uranium adsorption: a mini review of recent developments, *Front. Mater.*, 2025, 12.

28 M.-U.-D. Naik, Adsorbents for the uranium capture from seawater for a clean energy source and environmental safety: A Review, *ACS Omega*, 2024, **9**(11), 12380.

29 A. S. A. Ahmed, W. Xiang, I. Saana Amiinu and X. Zhao, Zeolitic-imidazolate-framework (ZIF-8)/PEDOT:PSS composite counter electrode for low cost and efficient dye-sensitized solar cells, *New J. Chem.*, 2018, **42**(21), 17303.

30 N. Yang, L. Lu, L. Zhu, P. Wu, D. Tao, X. Li, J. Gong, L. Chen, Y. Chao and W. Zhu, Phosphomolybdic acid encapsulated in ZIF-8-based porous ionic liquids for reactive extraction desulfurization of fuels, *Inorg. Chem. Front.*, 2022, **9**(1), 165.

31 L. Zhang, T. Mi, M. A. Ziaee, L. Liang and R. Wang, Hollow POM@MOF hybrid-derived porous $Co_3O_4/CoMoO_4$ nanocages for enhanced electrocatalytic water oxidation, *J. Mater. Chem. A*, 2018, **6**(4), 1639.

32 J. Tang, R. R. Salunkhe, J. Liu, N. L. Torad, M. Imura, S. Furukawa and Y. Yamauchi, Thermal conversion of core-shell metal-organic frameworks: a new method for selectively functionalized nanoporous hybrid carbon, *J. Am. Chem. Soc.*, 2015, **137**(4), 1572.

33 A. Subhadarshini, S. K. Samal, A. Pattnaik and B. Nanda, Facile fabrication of plasmonic Ag/ZIF-8: an efficient catalyst for investigation of antibacterial, haemolytic and photocatalytic degradation of antibiotics, *RSC Adv.*, 2023, **13**(45), 31756.

34 R. S. Malkar and G. D. Yadav, Synthesis of cinnamyl benzoate over novel heteropoly acid encapsulated ZIF-8, *Appl. Catal., A*, 2018, **560**, 54.

35 Q. Wang, E. Liu, C. Zhang, S. Huang, Y. Cong and Y. Zhang, Synthesis of $Cs_3PMo_{12}O_{40}/Bi_2O_3$ composite with highly enhanced photocatalytic activity under visible-light irradiation, *J. Colloid Interface Sci.*, 2018, **516**, 304.

36 H. Si, L. Sun, Y. Zhang, Y. Zhang, L. Bai and Y. Zhang, Carbon-coated MoO_2 nanoclusters anchored on rGO sheets as high-performance electrodes for symmetric supercapacitors, *Dalton Trans.*, 2019, **48**(1), 285.

37 X. Chen, X. Wang and D. Fang, A review on C1s XPS-spectra for some kinds of carbon materials, *Fullerenes, Nanotubes Carbon Nanostruct.*, 2020, **28**(12), 1048.

38 S. Yang, Y. Wang, H. Li, Y. Zhan, X. Ding, M. Wang, X. Wang and L. Xiao, Synthesis of nano-ZIF-8@chitosan microspheres and its rapid removal of p-hydroxybenzoic acid from the agro-industry and preservatives, *J. Porous Mater.*, 2021, **28**(1), 29.

39 W. Qi, H. Zhao, Y. Wu, H. Zeng, T. Tao, C. Chen, C. Kuang, S. Zhou and Y. Huang, Facile Synthesis of Layer Structured GeP_3/C with stable chemical bonding for enhanced lithium-ion storage, *Sci. Rep.*, 2017, **7**(1), 43582.

40 R. Yang, X. Yan, Y. Li, X. Zhang and J. Chen, Nitrogen-doped porous carbon-zno nanopolyhedra derived from ZIF-8: new materials for photoelectrochemical biosensors, *ACS Appl. Mater. Interfaces*, 2017, **9**(49), 42482.

41 A. A. Al-Ghamdi, A. A. Galhoum, A. Alshahrie, Y. A. Al-Turki, A. M. Al-Amri and S. Wageh, *Polymers*, 2023, **15**(5), 1157.

42 R. Foroutan, R. Mohammadi, A. Ahmadi, G. Bikhabar, F. Babaei and B. Ramavandi, Impact of ZnO and Fe_3O_4 magnetic nanoscale on the methyl violet 2B removal efficiency of the activated carbon oak wood, *Chemosphere*, 2022, **286**, 131632.

43 S. Wong, N. A. Ghafar, N. Ngadi, F. A. Razmi, I. M. Inuwa, R. Mat and N. A. S. Amin, Effective removal of anionic textile dyes using adsorbent synthesized from coffee waste, *Sci. Rep.*, 2020, **10**(1), 2928.

44 C. K. Enenebeaku, N. J. Okorocha, U. E. Enenebeaku and I. C. Ukaga, Adsorption and equilibrium studies on the removal of methyl red from aqueous solution using white potato peel powder, *Int. Lett. Chem., Phys. Astron.*, 2017, **72**, 52.

45 Y. Liu, C. Luo, J. Sun, H. Li, Z. Sun and S. Yan, Enhanced adsorption removal of methyl orange from aqueous solution by nanostructured proton-containing δ-MnO_2, *J. Mater. Chem. A*, 2015, **3**(10), 5674.

46 A. S. A. Ahmed, M. M. S. Sanad, A. Kotb, A. N. R. M. Negm and M. H. Abdallah, Removal of methyl red from wastewater using a NiO@Hyphaene thebaica seed-derived porous carbon adsorbent: kinetics and isotherm studies, *Mater. Adv.*, 2023, **4**(14), 2981.

47 Y. S. Ho and G. McKay, A Comparison of chemisorption kinetic models applied to pollutant removal on various sorbents, *Process Saf. Environ. Prot.*, 1998, **76**(4), 332.

48 R.-L. Tseng, P.-H. Wu, F.-C. Wu and R.-S. Juang, A convenient method to determine kinetic parameters of adsorption processes by nonlinear regression of pseudo-nth-order equation, *Chem. Eng. J.*, 2014, **237**, 153.

49 T. Shahwan, Sorption kinetics: Obtaining a pseudo-second order rate equation based on a mass balance approach, *J. Environ. Chem. Eng.*, 2014, **2**(2), 1001.

50 M. Gao, D. Xu, Y. Gao, G. Chen, R. Zhai, X. Huang, X. Xu, J. Wang, X. Yang and G. Liu, Mussel-inspired triple bionic adsorbent: Facile preparation of layered double hydroxide@polydopamine@metal-polyphenol networks and their selective adsorption of dyes in single and binary systems, *J. Hazard. Mater.*, 2021, **420**, 126609.

51 G. P. Jeppu and T. P. Clement, A modified Langmuir-Freundlich isotherm model for simulating pH-dependent adsorption effects, *J. Contam. Hydrol.*, 2012, **129–130**, 46.

52 C. G. Ramos, S. A. Sousa, A. M. Grilo, J. R. Feliciano, J. H. Leitão, *et al.*, The second RNA chaperone, Hfq_2, is also required for survival under stress and full virulence of Burkholderia cenocepacia J2315, *J. Bacteriol.*, 2014, **196**(22), 3980.

53 M. Alizadeh, S. J. Peighambardoust, R. Foroutan, H. Azimi and B. Ramavandi, Surface magnetization of hydrolyzed luffa cylindrica biowaste with cobalt ferrite nanoparticles for facile Ni^{2+} removal from wastewater, *Environ. Res.*, 2022, **212**, 113242.

54 R. H. Althomali, K. A. Alamry, M. A. Hussein and R. M. Guedes, An investigation on the adsorption and removal performance of a carboxymethylcellulose-based 4-aminophenazone@MWCNT nanocomposite against crystal violet and brilliant green dyes, *RSC Adv.*, 2023, **13**(7), 4303.

55 K. Zhang, C. Tang, H. Chen, P. Mao, G. Feng and C. Cai, Surface adsorption and bioreduction of uranium in low-concentration uranium-containing wastewater induced by Jonesia quinghaiensis ZFSY-01, *J. Water Process Eng.*, 2025, **70**, 107062.

56 A. Hamed, A. Orabi, H. Salem, D. Ismaiel, G. Saad, I. Abdelhamid, A. Elwahy and M. Elsabee, An effective uranium removal using diversified synthesized cross-linked chitosan bis-aldehyde Schiff base derivatives from

aqueous solutions, *Environ. Sci. Pollut. Res.*, 2023, **30**(49), 106790.

57 S. S. Hosseini, A. Hamadi, R. Foroutan, S. J. Peighambardoust and B. Ramavandi, Decontamination of Cd^{2+} and Pb^{2+} from aqueous solution using a magnetic nanocomposite of eggshell/starch/Fe_3O_4, *J. Water Process Eng.*, 2022, **48**, 102911.

58 M. A. Usman and A. Y. Khan, Selective adsorption of anionic dye from wastewater using polyethyleneimine based macroporous sponge: Batch and continuous studies, *J. Hazard. Mater.*, 2022, **428**, 128238.

59 R. Ding, Y. Zhu, L. Jing, S. Chen, J. Lu and X. Zhang, Sulfhydryl functionalized chitosan-covalent organic framework composites for highly efficient and selective recovery of gold from complex liquids, *Int. J. Biol. Macromol.*, 2024, **282**, 137037.

60 S. Chen, R. Ding, B. Li, J. Lu and X. Zhang, A robust aerogel incorporated with phthalocyanine-based porous organic polymers for highly efficient gold extraction, *Sep. Purif. Technol.*, 2025, **354**, 129451.

61 L. Yin, Y. Hu, R. Ma, T. Wen, X. Wang, B. Hu, Z. Yu, T. Hayat, A. Alsaedi and X. Wang, Smart construction of mesoporous carbon templated hierarchical Mg-Al and Ni-Al layered double hydroxides for remarkably enhanced U(VI) management, *Chem. Eng. J.*, 2019, **359**, 1550.

62 J. Wu, N. Shi, N. Li and Z. Wang, Dual-ligand ZIF-8 bearing the cyano group for efficient and selective uranium capture from seawater, *ACS Appl. Mater. Interfaces*, 2023, **15**(40), 46952.

63 K. Kuntaiah, A. M. Thomas, M. V. Rajavarapu, M. R. Korra and S. S. Nandakishore, Remediation of uranium from groundwater: characterization and utilization of activated carbon modified with aluminum and calcium phosphate, *J. Radioanal. Nucl. Chem.*, 2025, DOI: **10.1007/s10967-025-10332-7**.

64 M. A. Mahmoud, Kinetics studies of uranium sorption by powdered corn cob in batch and fixed bed system, *J. Adv. Res.*, 2016, **7**(1), 79.

65 C. Zhao, J. Liu, Y. Deng, Y. Tian, G. Zhang, J. Liao, J. Yang, Y. Yang, N. Liu and Q. Sun, Uranium (VI) adsorption from aqueous solutions by microorganism-graphene oxide composites *via* an immobilization approach, *J. Cleaner Prod.*, 2019, **236**, 117624.